J|A|C|S
ARTICLES
Published on Web 03/08/2003

Molecular and Electronic Structures of Iron Complexes Containing N,S-Coordinated, Open-Shell *o*-Iminothionebenzosemiquinonate(1−) π Radicals

Prasanta Ghosh, Eckhard Bill,* Thomas Weyhermüller, and Karl Wieghardt*

Contribution from the Max-Planck-Institut für Strahlenchemie, Stiftstrasse 34-36, D-45470 Mülheim an der Ruhr, Germany

Received December 4, 2002; E-mail: wieghardt@mpi-muelheim.mpg.de

Abstract: The reaction of the dinuclear species (μ-NH,NH)[$Fe^{III}(L^{IP})(L^{AP})$]$_2$ dissolved in CH_2Cl_2 with dioxygen affords black microcrystals of diamagnetic (μ-S,S)[$Fe^{III}(L^{IP})(L^{ISQ})$]$_2$·*n*-hexane (**6**) upon the addition of *n*-hexane, where $(L^{IP})^{2-}$ represents the dianion of 4,6-di-*tert*-butyl-2-aminothiophenol, $(L^{AP})^-$ is the corresponding monoanion, and $(L^{ISQ})^-$ is the corresponding *o*-iminothionebenzosemiquinonate(1−) π radical monoanion; similarly, the dianion $('H_2N_2S_2')^{2-}$ is derived from 1,2-ethanediamine-*N,N*′-bis(2-benzenethiol), and $('N_2S_2^{\bullet\prime})^{3-}$ is its monoradical trianion. The above reaction in a CH_2Cl_2/CH_3OH (1:1) mixture yields the diamagnetic isomer (μ-NH,NH)[$Fe^{III}(L^{IP})(L^{ISQ})$]$_2$·5$CH_3OH$ (**7**), whereas air oxidation of (μ-S,S)[$Fe^{II}('H_2N_2S_2')$]$_2$ in CH_3CN yields diamagnetic (μ-S,S)[$Fe^{III}('N_2S_2^{\bullet\prime})$]$_2$ (**8**). Complexes **6** and **8** were shown to undergo addition reactions with phosphines, phosphites, or cyanide affording the following complexes: *trans*-[$Fe^{II}(L^{ISQ})_2$-($P(OPh)_3$)] (**9**; $S_t = 0$) and [$N(n\text{-}Bu)_4$][$Fe^{II}(L^{ISQ})_2(CN)$] ($S_t = 0$). Oxidation of **6** in CH_2Cl_2 with iodine, bromine, and chlorine respectively yields black microcrystals of [$Fe^{III}(L^{ISQ})_2X$] (X = I, Br, or Cl) with $S_t = {}^1/_2$. The structures of complexes **6**−**9** have been determined by X-ray crystallography at 100 K. The oxidation level of the ligands and iron ions in all complexes has been unequivocally established, as indicated by crystallography; electron paramagnetic resonance, UV−vis, and Mössbauer spectroscopies; and magnetic-susceptibility measurements. The N,S-coordinated *o*-iminothionebenzosemiquinonate(1−) π radicals have been identified in all new complexes. The electronic structures of the new complexes have been determined, and it is shown that no evidence for iron oxidation states >III is found in this chemistry.

Introduction

It has recently[1,2] been realized that N,S-coordinated *o*-aminothiophenolate ligands belong to the class of noninnocent ligands. Three entities that differ in their protonation and oxidation levels[3] have been identified unequivocally as shown in Scheme 1, the most interesting one being the *o*-iminothionebenzosemiquinonate(1−) π radical.[1] The evidence presented rests predominantly on small but significant structural differences of the coordinated ligands, which are clearly detectable by high-quality, single-crystal X-ray crystallography where the experimental error of a given C−S, C−C, or C−N bond length should not exceed ±0.015 Å (3σ).[1] Scheme 2 shows the average bond distances in N,S-coordinated $(L^{AP})^-$, $(L^{IP})^{2-}$, and $(L^{ISQ})^{\bullet-}$ ligands.

In the present paper, we use the two ligands 4,6-di-*tert*-butyl-2-aminothiophenol,[4] H[L^{AP}], and 1,2-ethanediamine-*N,N*′-bis-(2-benzenethiol),[5] $'H_4N_2S_2'$ (Scheme 1). The coordination chemistry of $'H_4N_2S_2'$ with iron has been investigated in some detail by Sellmann and co-workers,[6,7] who reported complexes of the type [$Fe^{IV}('N_2S_2')(PR_3)$] and [$Fe^{V}('N_2S_2')I$] where the high formal oxidation states of +IV and +V of the iron ions had been derived by considering the closed-shell, tetraanionic ligand $('N_2S_2')^{4-}$ present in these complexes. In contrast, we recently presented evidence[2] that the spectroscopic oxidation states of the iron ions in these compounds are actually either +II (d,[6] low spin, $S_t = 0$) or +III (d,[5] intermediate spin, $S_{Fe} = {}^3/_2$) and that the ligands are, in both cases, open-shell diradical dianions $('N_2S_2^{\bullet\bullet\prime})^{2-}$.

In a preceding paper[8] of this series, we have shown that the above two ligands form the following complexes with $Fe^{II}Cl_2$ using anaerobic or dioxygen-deficient reaction conditions: (μ-S,S)[$Fe^{II}(L^{AP})_2$]$_2$ (**2**), (μ-S,S)[$Fe^{II}('H_2N_2S_2')$]$_2$ (**3**), (μ-NH,NH)-[$Fe^{III}(L^{IP})(L^{AP})$]$_2$ (**5a**), and (μ-S,S)[$Fe^{III}(L^{AP})(L^{IP})$]$_2$ (**5b**). These compounds were shown to contain only the closed-shell ligands $(L^{AP})^-$, $(L^{IP})^{2-}$, and $('H_2N_2S_2')^{2-}$ and a high-spin ferrous ion ($S_{Fe} = 2$) in **2** and **3** that are intramolecularly antiferromagnetically coupled, yielding the observed diamagnetic ground state ($S_t = 0$). In the isomers **5a** and **5b**, again the closed-shell,

(1) Herebian, D.; Bothe, E.; Bill, E.; Weyhermüller, T.; Wieghardt, K. *J. Am. Chem. Soc.* **2001**, *123*, 10012.
(2) Chun, H.; Weyhermüller, T.; Bill, E.; Wieghardt, K. *Angew. Chem., Int. Ed.* **2001**, *40*, 2489.
(3) Holm, R. H.; O'Connor, M. J. *Prog. Inorg. Chem.* **1971**, *14*, 241.
(4) Sellmann, D.; Käppler, O. *Z. Naturforsch., B: Chem. Sci.* **1987**, *42b*, 1291.
(5) Sellmann, D.; Käppler, O.; Knoch, F.; Moll, M. *Z. Naturforsch. B: Chem. Sci.* **1990**, *45b*, 803.
(6) Sellmann, D.; Emig, S.; Heinemann, F. W.; Knoch, F. *Angew. Chem., Int. Ed. Engl.* **1997**, *36*, 1201.
(7) Sellmann, D.; Emig, S.; Heinemann, F. W. *Angew. Chem., Int. Ed. Engl.* **1997**, *36*, 1734.
(8) Ghosh, P.; Begum, A.; Bill, E.; Weyhermüller, T.; Wieghardt, K. *Inorg. Chem.*, in press.

Scheme 1. Ligands and Abbreviations

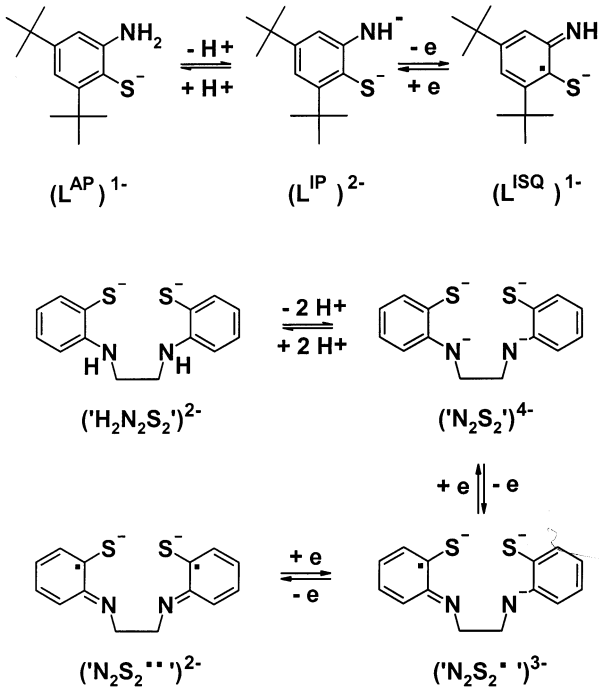

Scheme 2. Bond Distances (Å) in N,S-Coordinated Ligands

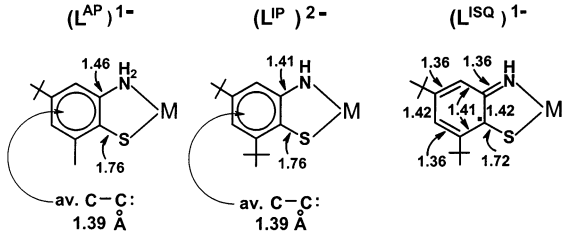

N,S-coordinated ligands $(L^{AP})^-$ and $(L^{IP})^{2-}$ prevail, and the central ferric ion was shown to possess a local intermediate-spin electron configuration, $S_{Fe} = {}^3/_2$, which, in the dimers, couples strongly and antiferromagnetically, also yielding a diamagnetic ground state ($S_t = 0$). Complexes **2** and **5a** have been studied by single-crystal X-ray crystallography.

Complexes **5a** and **5b** in CH_2Cl_2 solutions were found to be sensitive to dioxygen. Here we report on the oxidation products obtained from such solutions. We will study in detail the molecular and electronic structures of ferrous and ferric complexes containing *o*-iminothionebenzosemiquinonate π radicals. We also use stronger oxidants than dioxygen such as iodine, bromine, or chlorine. Scheme 3 shows the complexes prepared.

We use the same labeling system for the compounds introduced in ref 8, which may be considered to be part one of the present investigation. Thus, complexes **1**−**4** and **5a** and **5b** are described in ref 8, whereas complexes **6**−**10** and **11a**−**c** will be presented here.

Experimental Section

The ligands $H[L^{AP}]$[4] and $''H_4N_2S_2'$[5] were prepared according to published procedures. Complexes **5a** and $[Fe^{II}('N_2S_2^{\bullet\bullet}')(PPh_3)]$ have been synthesized as described in refs 8 and 6, respectively.

(μ-S,S)[$Fe^{III}(L^{IP})(L^{ISQ})$]$_2$·*n*-hexane (6). A solution of **5a** (0.20 g, 0.38 mmol) in CH_2Cl_2 (40 mL) was stirred in the presence of air at ambient temperature for a few minutes. To the dark-blue solution was added 20 mL of *n*-hexane. The solvents were allowed to slowly evaporate under an argon atmosphere, whereupon dark brown-black crystals of **6**·*n*-hexane formed. Yield: 0.20 g (92%). IR (KBr disk) ν(N−H): 3332, 3313 cm^{-1}. Anal. Calcd for $C_{56}H_{84}Fe_2N_4S_4$·*n*-hexane: C, 65.38; H, 8.68; N, 4.92; S, 11.25; Fe, 9.84. Found: C, 65.3; H, 8.7; N, 4.9; S, 11.3; Fe, 9.8.

Scheme 3. Complexes Prepared

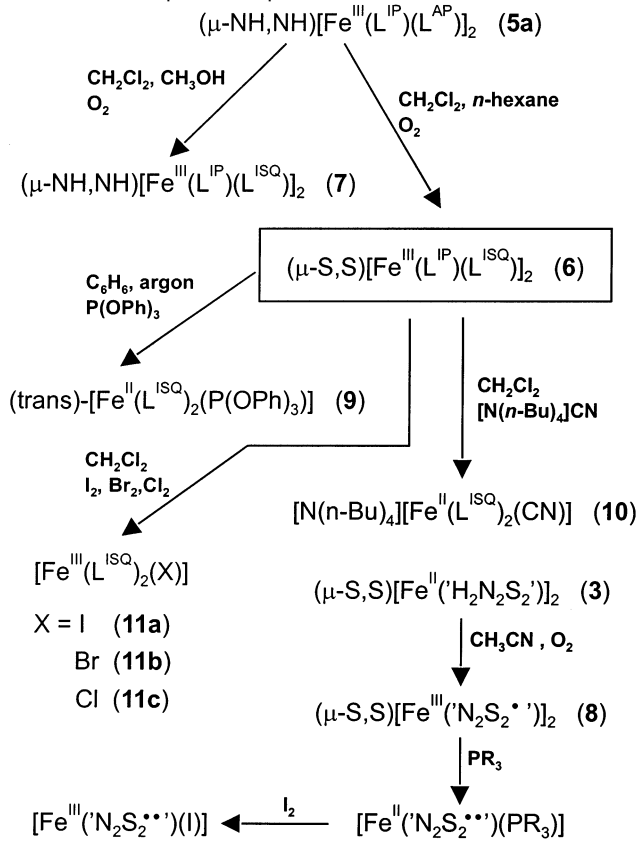

(μ-NH,NH)[$Fe^{III}(L^{IP})(L^{ISQ})$]$_2$·5$CH_3OH$ (7). A solution of **5a** (0.21 g, 0.2 mmol) in CH_2Cl_2 (40 mL) was briefly exposed to air at 20 °C with stirring until a deep-blue solution was obtained. This solution was quickly purged with argon, and methanol (20 mL) was added. The solvents were allowed to slowly evaporate under argon. Dark brown-black crystals of **7** precipitated and were filtered off. Yield: 0.20 g (83%). After the removal of the crystals from the solvent, they rapidly lose one methanol molecule of crystallization with the destruction of the crystalline habitus. All spectroscopic investigations were carried out on powder samples of (μ-NH,NH)[$Fe^{III}(L^{AP}-H)(L^{ISQ})$]$_2$·4$CH_3OH$ only, and for the crystal structure determination, a crystal of **7** was used. IR (KBr disk) ν(N−H): 3292, 3277 cm^{-1}. Anal. Calcd for $C_{56}H_{84}Fe_2N_4S_4$·4CH_3OH: C, 61.01; H, 8.47; N, 4.74; S, 10.85; Fe, 9.49. Found: C, 60.6; H, 8.6; N, 4.9; S, 10.9; Fe, 9.5.

(μ-S,S)[$Fe^{III}('N_2S_2^{\bullet\prime})$]$_2$ (8). To a degassed solution of the ligand $'H_4N_2S_2'$ (0.60 g, 2.2 mmol) in dry CH_3CN (40 mL) was added under an argon-blanketing atmosphere $FeCl_2$ (0.254 g, 2.0 mmol). To this mixture was added dropwise with stirring under argon triethylamine (3.5 mmol). After stirring for 2 h at 20 °C, crystalline yellow **3** precipitated. Upon filtration of this material in the presence of air, the color of the solid turned immediately black. The black material was washed repeatedly with dry CH_3CN and, finally, was recrystallized from a CH_2Cl_2/*n*-hexane mixture (2:1; 40 mL, 200-mg complex) under argon as black crystals of (μ-S,S)[$Fe^{II}('N_2S_2^{\bullet\bullet})$]$_2$·$^5/_6CH_2Cl_2$. Yield: 0.56 g (85%). Anal. Calcd for $C_{28}H_{28}N_4S_4Fe_2$·$^5/_6CH_2Cl_2$: C, 47.93; H, 3.57; N, 7.70; Fe, 15.40. Found: C, 48.2; H, 3.4; N, 7.9; Fe, 14.9.

[$Fe^{II}(L^{ISQ})_2(P(OPh)_3)$] (9). To a solution of **5a** (0.22 g, 0.20 mmol) in benzene (30 mL) under an argon-blanketing atmosphere was added triphenyl phosphite (0.16 g, 0.50 mmol) with stirring for 15 min at 20

Table 1. Crystallographic Data for **6**·C_6H_{14}, **7**·5CH_3OH, **8**·5/6CH_2Cl_2, and **9**·$C_6H_5CH_3$

	6·C_6H_{14}	**7**·5CH_3OH	**8**·5/6CH_2Cl_2	**9**·$C_6H_5CH_3$
chemical formula	$C_{62}H_{98}Fe_2N_4S_4$	$C_{61}H_{104}Fe_2N_4O_5S_4$	$C_{28.83}H_{25.67}Cl_{1.67}Fe_2N_4S_4$	$C_{53}H_{65}FeN_2O_3PS_2$
fw	1139.38	1213.42	727.22	929.01
space group	$P\bar{1}$, No. 2	$P\bar{1}$, No. 2	$P\bar{1}$, No. 2	*Aba*2, No. 41
a, Å	10.539(5)	10.6112(9)	13.9882(8)	28.436(2)
b, Å	11.343(5)	10.6514(9)	16.4986(10)	17.4172(9)
c, Å	14.532(6)	16.910(2)	20.688(2)	9.9671(6)
α, deg	103.94(2)	73.80(2)	70.96(1)	90
β, deg	101.98(2)	76.29(2)	75.89(1)	90
γ, deg	99.29(2)	66.93(2)	75.30(1)	90
V, Å	1607.9(12)	1670.8(3)	4297.3(5)	4936.5(5)
Z	1	1	6	4
T, K	100(2)	100(2)	100(2)	100(2)
ρ^{calcd}, g cm^{-3}	1.177	1.206	1.686	1.250
diffractometer used	Siemens SMART	Nonius Kappa-CCD	Nonius Kappa-CCD	Nonius Kappa-CCD
reflns collected/Θ_{max}	6322/23.27	13 640/27.50	24 954/22.50	15 790/27.50
unique reflns/$I > 2\sigma(I)$	4519/2891	7442/5408	10 969/7136	5187/4170
no. of params/restraints	343/31	378/1	1097/18	257/1
μ(Mo Kα), cm^{-1}	6.19	6.04	14.89	6.70
R1[a]/goodness of fit[b]	0.0757/1.039	0.0595/1.040	0.0671/1.027	0.0516/1.048
wR2[c] [$I > 2\sigma(I)$]	0.1897	0.1405	0.1327	0.0936

[a] Observation criterion: $I > 2\sigma(I)$. R1 $=\sum||F_o| - |F_c||/\sum|F_o|$. [b] GOF $= \{\sum[w(F_o^2 - F_c^2)^2]/(n-p)\}^{1/2}$. [c] wR2 $= \{\sum[w(F_o^2 - F_c^2)^2]/\sum[w(F_o^2)^2]\}^{1/2}$ where $w = 1/\sigma^2(F_o^2) + (aP)^2 + bP$, $P = (F_o^2 + 2F_c^2)/3$.

°C. The dark-blue color of the solution immediately turned to dark green. The reaction volume was reduced to half by evaporation of the solvent in vacuo. To the dark-green solution was added *n*-hexane (20 mL). Slow evaporation of the solvent mixture produced dark-green crystals of **9**. Yield: 0.19 g (57%). IR (KBr disk) ν(N−H): 3296 cm^{-1}. Anal. Calcd for $C_{46}H_{57}O_3N_2PS_2Fe$: C, 66.0; H, 6.81; N, 3.34; S, 7.65; P, 3.70. Found: C, 64.8; H, 6.6; N, 3.2; S, 7.8; P, 3.5. Crystals of **9**·toluene were grown from a solution of **9** in toluene by slow evaporation of the solvent.

[N(*n*-Bu)$_4$][Fe^{II}(L^{ISQ})$_2$(CN)] (10). To a solution of **6** (0.11 g, 0.10 mmol) in dry benzene (40 mL) was added dropwise with stirring under argon a solution of [N(*n*-Bu)$_4$]CN (0.055 g, 0.19 mmol) in benzene (20 mL), whereupon the blue color of the solution changed to dark green. After removal of the solvent by evaporation under reduced pressure until 15−20 mL was left over, dry *n*-hexane (15 mL) was added under argon. A dark-green, microcrystalline precipitate formed within 30 min that was filtered off, strictly under argon, and washed with *n*-hexane. Yield: 85 mg (53%). ESI−MS: (positive ion) 242 [N(*n*-Bu)$_4$]$^+$, (negative ion) 552 [M]. Anal. Calcd for $C_{44}H_{78}N_3S_2Fe$: C, 68.00; H, 9.90; N, 7.05; S, 8.06. Found: C, 67.8; H, 10.1; N, 6.8; S, 7.9. IR (KBr disk) ν(CN): 2084 cm^{-1}.

[Fe^{III}(L^{ISQ})$_2$I] (11a). To a solution of **6** (0.22 g, 0.20 mmol) in CH_2Cl_2 (40 mL) was added under an argon atmosphere with stirring at ambient temperature iodine (0.05 g, 0.20 mmol) dissolved in *n*-hexane (25 mL). The color of the solution slowly changed from dark blue to dark violet. After stirring for an additional 20 min, the solvent was removed in vacuo. To the residue was added *n*-hexane (20 mL). After filtration, the residual brown microcrystalline product was dissolved in CH_2Cl_2 (40 mL) under argon. Addition of *n*-hexane (25 mL) and evaporation of the solvents under reduced pressure yielded ∼0.20 g of **11a** (77%) as brown microcrystals. IR (KBr disk) ν(N−H): 3231 cm^{-1}. Anal. Calcd for $C_{28}H_{42}N_2S_2FeI$: C, 51.45; H, 6.43; N, 4.28; S, 9.80; I, 19.45; Fe, 8.57. Found: C, 51.3; H, 6.3; N, 4.2; S, 9.85; I, 19.6; Fe, 8.6.

[Fe^{III}(L^{ISQ})$_2$Br] (11b) and [Fe(L^{ISQ})$_2$Cl] (11c). To a solution of **6** (0.11 g, 0.10 mmol) in benzene (30 mL) was added dropwise with stirring under argon a 10-mm solution of bromine in *n*-hexane (10−12 mL) or, alternatively, a dilute solution of chlorine in *n*-hexane. In both cases, the dark-blue color of the solutions turned rapidly to dark violet. The solvent was immediately evaporated under reduced pressure. To the corresponding residue was added *n*-hexane (10 mL), and the mixture was stirred. A dark-brown microcrystalline material was collected by filtration. Yield: 50−60% with respect to the precursor complex. IR (KBr disk) ν(NH): (**11b**) 3220, 3198 cm^{-1}; (**11c**) 3224, 3190 cm^{-1}. Anal. Calcd for $C_{28}H_{42}N_2S_2FeBr$: C, 55.45; H, 6.93; N, 4.62; S, 10.56; Br, 13.20; Fe, 9.24. Found: C, 55.6; H, 7.0; N, 4.6; S, 10.4; Br, 13.1; Fe, 9.1. Anal. Calcd for $C_{28}H_{42}N_2S_2FeCl$: C, 59.83; H, 7.48; N, 4.98; S, 11.40; Cl, 6.32; Fe, 9.97. Found: C, 59.7; H, 7.4; N, 4.8; S, 11.6; Cl, 6.4; Fe, 9.9.

X-ray Crystallographic Data Collection and Refinement of the Structures. Single black crystals of **6**−**9** were coated with perfluoropolyether, picked up with a glass fiber, and immediately mounted in the nitrogen cold streams of the diffractometers to prevent the loss of solvent. Intensity data were collected at 100 K using graphite-monochromated Mo Kα radiation ($\lambda = 0.710\,73$ Å). Final cell constants were obtained from a least-squares fit of a subset of several thousand strong reflections. Data collection was performed by hemisphere runs, taking frames at 0.3° (Siemens SMART) and 1.0° (Nonius Kappa-CCD) in ω. Crystal faces were determined and the Gaussian-type correction routine embedded in ShelXTL[9] was used to account for absorption.[10] The 2θ cut-off limits of the data sets of **6** and **8** were set to 46.5° and 45°, respectively, because the small crystals diffracted only weakly. Crystallographic data of the compounds and diffractometer types used are listed in Table 1. The Siemens ShelXTL[9] software package was used for the solution, refinement, and artwork of the structure. The structures were readily solved by direct methods and difference Fourier techniques. All non-hydrogen atoms except some atoms in the disordered parts were refined anisotropically, and the hydrogen atoms attached to carbon atoms were placed at calculated positions and refined as riding atoms with isotropic displacement parameters. The hydrogens attached to nitrogen atoms were, where possible, located from the difference map and refined with restrained N−H distances using the SADI option. Disordered *tert*-butyl groups and solvent molecules were refined using a split-atom model with restrained distances.

Physical Measurements. The equipment used for IR, UV−vis, and Mössbauer spectroscopies has been described in refs 8 and 11. The temperature-dependent magnetic susceptibilities of solid samples of the complexes were measured by using a SQUID magnetometer (Quantum Design) at 1.0 T (2.0−300 K). Corrections for underlying diamagnetism

(9) *ShelXTL*, version 5; Siemens Analytical X-ray Instruments, Inc.: Madison, WI, 1994.
(10) Sheldrick, G. M. *SADABS*; Universität Göttingen: Göttingen, Germany, 1994.
(11) Meyer, K.; Bill, E.; Mienert, B.; Weyhermüller, T.; Wieghardt, K. *J. Am. Chem. Soc.* **1999**, *121*, 4859.

were made by using tabulated Pascal constants. The programs used for the simulation of Mössbauer and magnetization measurements on the basis of a spin Hamiltonian description are also described in ref 11 in detail. The X-band electron paramagnetic resonance (EPR) spectra were measured on frozen solutions by using a Bruker ELEXSYS E300 spectrometer with a standard or dual-mode cavity and an Oxford Instruments ESR 910 flow cryostat. Spin Hamiltonian simulations of compounds **11a** and **11b**, with total spin $S = {}^1/_2$, were performed with the XSOPHE program written by Hanson et al., which is distributed by Bruker Biospin GmbH. Ligand hyperfine interactions, including quadrupole interactions, were considered with the full-matrix approach.

Results and Discussion

Synthesis and Characterization of Complexes. 1. Complexes 6−8. It is a well-established observation that the yellow dinuclear complexes **1**−**3** containing two (μ-S,S)-bridged monomers, each with a central high-spin ferrous ion and two *o*-aminothiophenolato(1−)-type ligands, are very sensitive toward dioxygen both in solution and in the solid state.[8,12] The products are usually black powders that had not been investigated in detail previously.

We have also discovered that the oxidation of brown **5a** or **5b** in CH_2Cl_2 or CH_2Cl_2/CH_3OH (1:1) solutions with air yields black microcrystalline solids of **6** and **7**, eq 1. Similarly, the oxidation of yellow **3**[8] with dioxygen in acetonitrile or in the solid state without solvent yields black **8**, eq 2.

$$[Fe^{III}(L^{AP})(L^{IP})]_2 + {}^1/_2O_2 \rightarrow [Fe^{III}(L^{IP})(L^{ISQ})]_2 + H_2O \quad (1)$$

$$[Fe^{II}(L^{AP})_2]_2 + O_2 \rightarrow [Fe^{III}(L^{IP})(L^{ISQ})]_2 + 2H_2O \quad (2)$$

As we will show below from the X-ray structure determinations and Mössbauer spectroscopy, all three complexes **6**−**8** consist of dimers with two ferric ions, two terminal *o*-iminothionebenzosemiquinonato(1−) π radicals, and two bridging *o*-iminothiophenolato(2−) ligands (Scheme 1). Figure 1 shows the electronic spectra of these species in CH_2Cl_2 solution. Note the similarity of the spectra of **6**−**8**, all of which display a very intense ($\sim 10^4$ M^{-1} cm^{-1}) absorption in the visible range at 514 (**7**), 561 (**8**), and 571 (**6**) nm (Table 2).

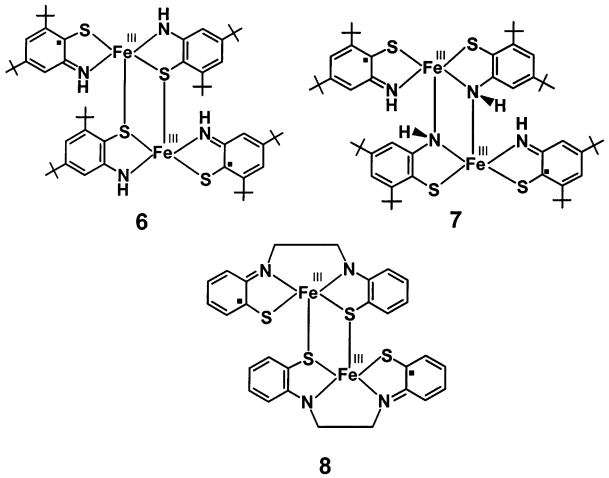

Temperature-dependent magnetic-susceptibility measurements using a SQUID magnetometer revealed that **6**−**8** possess a diamagnetic $S_t = 0$ ground state. Figure 2 shows the temperature dependence of the magnetic moments of **6** and **8**. Complex **6** clearly has an $S_t = 0$ ground state with a minor 5% paramagnetic impurity, and it exhibits a monotonically increasing magnetic moment, μ_{eff}, above 150 K. This behavior was successfully simulated with the assumption of two-exchange coupled subspins of $S^* = 1$ with a coupling constant of $J = -330$ cm^{-1} ($H = -2JS_1^*S_2^*$; $S_1^* = S_2^* = 1$). This model is physically meaningful because the Mössbauer parameters (see below) indicate a local spin at the iron ion in **6**−**8** of $S_{Fe} = {}^3/_2$, which is strongly intramolecularly coupled to one N,S-coordinated *o*-iminothionebenzosemiquinonate(1−) π radical per iron ion, yielding the fictitious subspin of $S^* = 1$.

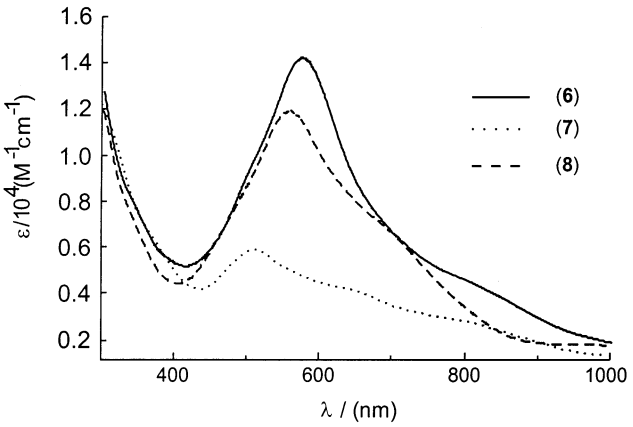

Figure 1. Electronic spectra of **6** (CH_2Cl_2), **7** (1:1 CH_2Cl_2/CH_3OH), and **8** (CH_2Cl_2).

Table 2. Electronic Spectra of Complexes

complex	conditions[a]	λ_{max}, nm (ϵ^b, 10^4 M^{-1} cm^{-1})
5a	a	600 br (0.23), 766 br (0.13)
5b	b	504 br (0.26)
6	c	571 (1.4), 800 sh (0.46)
7	d	514 (0.58), 670 sh (0.38), 800 sh (0.27)
8	c	561 (1.2), 700 (0.65)
9	e	320 sh (0.85), 437 (0.84), 525 sh (0.4), 690 (2.4)
10	a	380 sh (0.48), 460 (0.60), 620 sh (0.6), 709 (0.98)
11a	c	350 (1.1), 475 sh (1.5), 558 (3.6), 780 sh (0.23)
11b	c	350 (0.87), 475 sh (0.87), 541 (2.0), 780 sh (0.15)
11c	a	350 (1.2), 475 sh (0.82), 536 (2.15), 750 sh (0.13)

[a] Conditions: (a) strictly under argon in toluene solution; (b) under argon in CH_3CN; (c) in CH_2Cl_2; (d) in a CH_2Cl_2/CH_3OH (1:1, v/v) mixture; (e) in the presence of 5 mmol of $P(OPh)_3$ in CH_2Cl_2. [b] Extinction coefficients are calculated per iron ion.

It is interesting that **6** and **7** are geometrical isomers. In **6**, the two ligands $(L^{IP})^{2-}$ and $(L^{ISQ})^-$ are coordinated in a trans fashion relative to each other, whereas in **7**, it is cis. As a consequence of this, the two monomers form the respective dimer via two μ-thiolato bridges in **6** but via two μ-imino bridges in **7**.

2. Complexes 9, 10, and $[Fe^{II}(^{\prime}N_2S_2^{\bullet\prime})(PR_3)]$. The dinuclear complexes **6**−**8** have subsequently been shown to form mononuclear adducts with phosphines, phosphites, or cyanide ligands. These mononuclear adducts invariably possess diamagnetic

(12) Larkworthy, L. F.; Murphy, J. M.; Phillips, D. J. *Inorg. Chem.* **1968**, *7*, 1436.

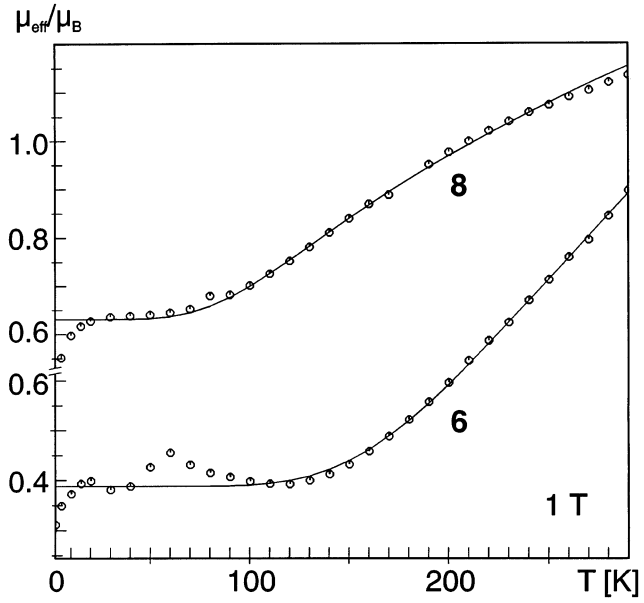

Figure 2. Temperature dependence of the magnetic moment, μ_{eff}, of the complexes of solid samples of **6** and **8** measured at 1 T. Spin Hamiltonian simulations (solid lines) for the exchange-coupled systems $S_1^* = 1$ and $S_2^* = 1$ with $H_{ex} = -2J^*S_1^*S_2^*$ and $J^* = -328$ cm^{-1} for **6** and -138 cm^{-1} for **8**. For **8** only, 50% of the sample is assumed to contribute to the paramagnetic signals. Other parameters: 5% impurity ($S = {}^1/_2$), 350×10^{-6} emu TIP (**6**); 13% impurity ($S = {}^1/_2$), 1370×10^{-6} emu TIP (**8**). The TIP contribution was subtracted from the experimental values.

ground states. Thus, the reaction of **6** in benzene under argon with triphenyl phosphite, $P(OPh)_3$, produced the dark-green microcrystalline solid of **9**. The same product was obtained using **5a** as the starting material and conducting the addition reaction in the presence of air. Similarly, when $[N(n\text{-}Bu)_4]CN$ was added to **6** dissolved in benzene under anaerobic conditions, dark-green microcrystals of **10** were obtained in good yields.

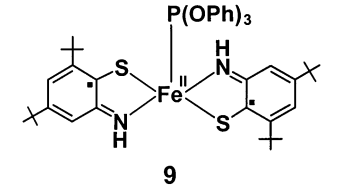

9

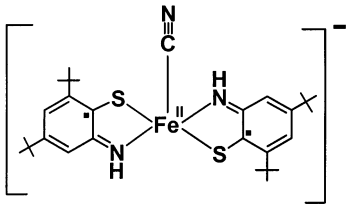

10

The electronic spectra of **9** and **10** in CH_2Cl_2 solution are shown in Figure 3; they are very similar and are dominated by a very intense ($>10^4$ M^{-1} cm^{-1}) absorption at 690 and 709 nm, respectively. They resemble closely the spectra reported by Sellmann et al.[6] for the structurally characterized species [Fe^{II}('$N_2S_2^{\bullet\bullet}$')(P(*n*-Pr)$_3$)] and [Fe^{II}('$N_2S_2^{\bullet\bullet}$')(PPh$_3$)]. From the magnetic-susceptibility measurements of **9** and **10** (3−300 K), it clearly

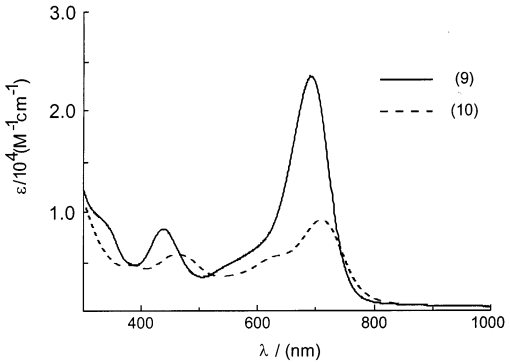

Figure 3. Electronic spectra of **9** and **10** in CH_2Cl_2.

follows that both compounds are diamagnetic ($S_t = 0$) even at room temperature.

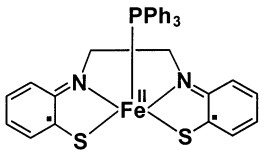

[Fe^{II}('$N_2S_2^{\bullet\bullet}$')(PPh$_3$)]
ref. [6]

This is remarkable because it has been reported in the literature[6] that the complexes [Fe('N_2S_2')(PR$_3$)] are paramagnetic and have an $S_t = 1$ ground state. To check these results, we have prepared [Fe('$N_2S_2^{\bullet\bullet}$')(PPh$_3$)] by following the published procedure,[6] which involves the reaction of the uncoordinated ligand Li('$H_2N_2S_2$') with ferrous dichloride and excess PPh$_3$ in THF/CH_3OH and air oxidation. It is also possible to generate this compound by the reaction of **8** with excess PPh$_3$ in CH_2Cl_2 under anaerobic conditions. Our samples crystallize in the same space group as those reported previously and have the same electronic spectrum as that reported in ref 6. It is noteworthy that our crude product displays a magnetic moment of ~2.4 μ_B at 298 K, which drops below 0.6 μ_B after two recrystallizations. The temperature dependence (3−298 K) of μ_{eff} of the crude sample obeys virtually a square-root behavior like temperature-independent paramagnetic (TIP) susceptibility. The magnitude of the moment, however, is found to be sample-dependent, and, therefore, it is not due to genuine TIP but to magnetic-particle contamination. Thus, Sellmann et al.'s [Fe^{II}('$N_2S_2^{\bullet\bullet}$')(PR$_3$)] complexes also possess a diamagnetic ground state, as does its isostructural ruthenium analogue [Ru^{II}('$N_2S_2^{\bullet\bullet}$')(PPh$_3$)].[13]

3. Complexes 11a−c and [Fe('$N_2S_2^{\bullet\bullet}$')I]. The reaction of complex **6** dissolved in CH_2Cl_2 with iodine, bromine, or chlorine yields dark-violet solutions from which the neutral complexes [Fe^{III}(L^{ISQ})$_2$X], with X = I (**11a**), Br (**11b**), or Cl (**11c**), were isolated as brown microcrystalline materials in good yields. These reactions are similar to that reported by Sellmann et al.,[7] who oxidized [Fe^{II}('$N_2S_2^{\bullet\bullet}$')(PR$_3$)] with I_2, yielding [Fe^{III}('$N_2S_2^{\bullet\bullet}$')I].

Figure 4 shows the electronic spectra of **11a−c** in CH_2Cl_2 solution. These spectra are very similar to that reported for [Fe^{III}('$N_2S_2^{\bullet\bullet}$')I]; they are dominated by a single intense ($>10^4$ M^{-1}

(13) Sellmann, D.; Ruf, R.; Knoch, F.; Moll, M. *Inorg. Chem.* **1995**, *34*, 4745.

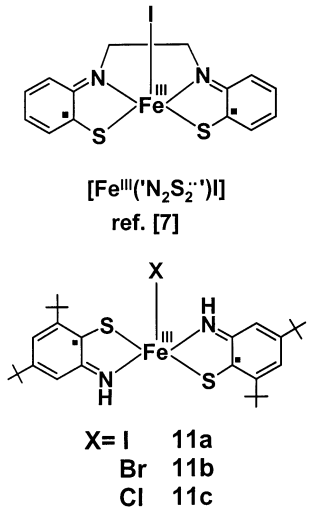

cm^{-1}) absorption in the range 560−540 nm. This maximum strongly resembles a charge-transfer (CT) transition observed for $[M^{II}(L^{ISQ})_2]$, with M = Ni, Pd, and Pt, at 837, 822, and 732 nm, respectively, which has been assigned to a spin- and dipole-allowed ligand-to-ligand CT transition.[1] Thus, the observation of this transition is a marker for the presence of two N,S-coordinated *o*-iminothionebenzosemiquinonato(1−) ligands.

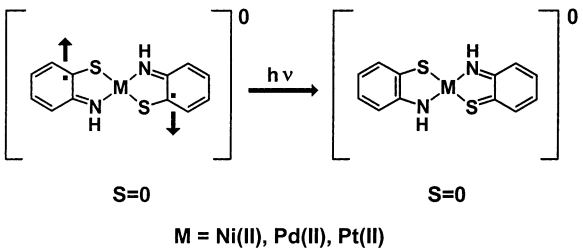

Figure 5 shows the effective magnetic moments of solid samples of **11a**−**c** measured at 1 T as a function of the temperature. The effective magnetic moments are close to the spin-only value of one unpaired electron and show virtually no temperature dependence above 100 K. Thus, excited spin states are not populated up to room temperature, and spin-coupling schemes for iron(III)-radical systems cannot be determined from the data. The solid lines in Figure 5 represent spin Hamiltonian simulations for $S_t = {}^1/_2$ systems, including some intermolecular-exchange interactions between molecules using Weiss' constant θ. The inset in Figure 5 shows an alternative simulation for these weak interactions for **11a** by using a dimer model, where two independent molecules, both with $S_t = {}^1/_2$, interact in the solid in an antiferromagnetic fashion (isotropic exchange $H_{ex} = -2J_m S_1 S_2$, $S_1 = S_2 = {}^1/_2$). A satisfactory fit has been obtained with the following parameters: $J_m = -3.5$ cm^{-1}, 0.8% paramagnetic impurity ($S = {}^5/_2$), and TIP $\chi_{TIP} = 525 \times 10^{-6}$ emu. This TIP contribution was subtracted from the experimental magnetic-susceptibility values. As pointed out above, the high TIP values for **11a** and **11b** (1180×10^{-6} emu) and **11c** (790×10^{-6} emu) are probably "effective" values that account for small impurities of single-domain magnetic particles (iron oxides) rather than genuine TIP values.

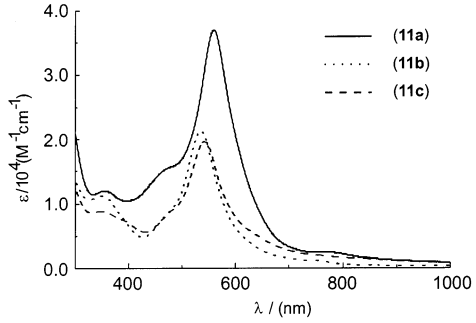

Figure 4. Electronic spectra of **11a**−**c** in CH_2Cl_2.

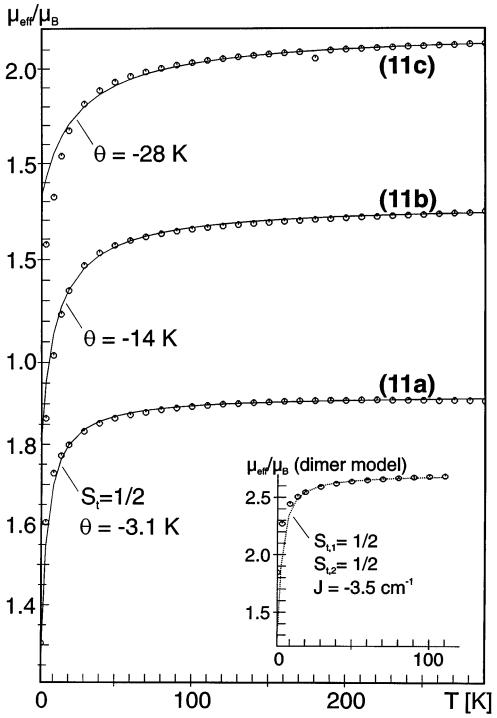

Figure 5. Effective magnetic moments of solid **11a**−**c** measured at 1 T as a function of the temperature and spin Hamiltonian simulations for $S = {}^1/_2$, including intermolecular interactions with Weiss constants θ_w (solid lines). The inset shows an alternative simulation for **11a** by using interacting molecule dimers (molar mass doubled) with $S_1 = {}^1/_2$ and $S_2 = {}^1/_2$ and isotropic exchange ($H_{ex} = -2J_m S_1 S_2$). Other parameters: 0.8% impurity ($S = {}^5/_2$), 525×10^{-6} emu TIP (**11a**); 118×10^{-6} emu TIP (**11b**); 1.2% impurity ($S = {}^5/_2$), 790×10^{-6} emu TIP (**11c**). The TIP contribution was subtracted from the experimental values. The high TIP values of **11a** and **11b** are probably "effective" values that account for the small impurities of single-domain ferromagnetic particles rather than genuine TIP values.

EPR Spectra. The X-band EPR spectra of **11a**−**c** in frozen CH_3CN solution at 10 K confirm the monomeric nature and the spin doublet ground state of these complexes (Figure 6). These spectra show well-resolved powder lines in the $g = 2$ region with strong anisotropy, which arises from spin−orbit interaction and indicates significant spin density at the iron sites. Unexpectedly, the spectra exhibit resolved hyperfine splittings at g_{min} with very unusual appearances. The splittings are largest for the iodine compound **11a** and small and unresolved for the chlorine compound **11c**. Because of the peculiar intensity distribution, the patterns seem, at first glance, to indicate hyperfine interaction with a number of ^{14}N and ^1H nuclei. However, satisfactory fits cannot be obtained with any reasonable number of (equal or unequal) nitrogen and protons sensing the spin density. In particular, the strong, apparently unsplit "central" hyperfine line at g_{min} in the spectrum of **11a** cannot be explained at all by using this model because ^{14}N and ^1H are

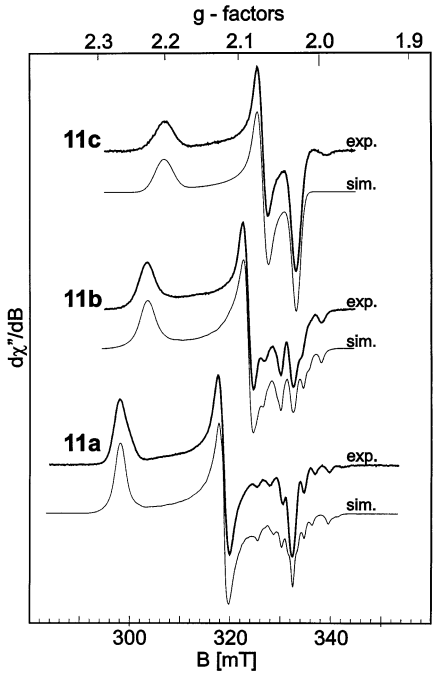

Figure 6. X-band EPR spectra of **11a**−**c** recorded at 10 K in frozen acetonitrile. Microwave frequency 9.4558 GHz/9.4563 GHz/9.4557 GHz; power 40 μW, modulation 0.9 mT/100 kHz. The simulations are described in the text, and the obtained parameters are summarized in Table 3.

100% isotopes. Instead, satisfactory simulations were obtained by adopting hyperfine interaction with a single apical halide ligand, which is ^{127}I ($I = {}^5/_2$; 100% natural abundance) for **11a** and ^{79}Br/^{81}Br ($I = {}^3/_2$; 50.7/49.3%) for **11b**, respectively.

The very unusual splitting and intensity pattern of the hyperfine lines owes its origin to *large electric quadrupole interactions* of the halide ligands, which mixes and shifts the m_I sublevels of the nuclear-spin manifolds. This affects the transition probabilities and even induces "forbidden" transitions with virtually $\Delta m_I > 0$, particularly with a nonzero anisotropy factor η. It is important to recall that the influence of quadrupole interactions on EPR hyperfine patterns results from higher-order effects. Reasonable simulations of the strong perturbations observed here require, therefore, that the electric-field-gradient (EFG) tensor of iodine and bromine be oriented "off" from the principal axes systems of the respective **A** tensor.

For **11a** and **11b**, the major components of the EFG coupling tensor **P** are found virtually in the direction of g_{max}, which is *perpendicular* to A_{max} (along g_{min}). As expected, along P_{max} only minor relative shifts of the respective hyperfine lines could be simulated, but the pronounced intensity modulation of the hyperfine pattern with a series of weak "satellite" lines could not be reproduced. The numerical values of the **g**, **A**, and **P** tensors obtained from the simulations are summarized in Table 3. The different strengths of the hyperfine splittings and the quadrupole perturbation can be understood as the effect of differing covalent iron−ligand interactions, which are further modulated by differing nuclear g factors and quadrupole moments (see Table 3).

Crystal Structure Determinations. The crystal structures of **6**−**9** have been determined by single-crystal X-ray crystallography at 100 K. Table 1 gives crystallographic data, and Table 4 summarizes important bond lengths. The structures of

Table 3. Spin Hamiltonian Parameters of **11a**−**c** from the EPR Simulations Shown in Figure 6[a]

	11a	11b	11c
g	2.264, 2.120, 2.032	2.225, 2.209, 2.032	
A[b], 10^{-4} cm^{-1}	3, 4, −19.1	6, 4, −24.0	
P[c], 10^{-4} cm^{-1}	−13.7, 8.1, 5.6	−11.9, 6.5, 5.4	
β[d], deg	11	18	
ligand nucleus	^{127}I	^{79}Br/^{81}Br	^{35}Cl/^{37}Cl
nuclear spin I	$^5/_2$	$^3/_2$	$^3/_2$
g_N[e]	1.13	14.0/1.51	0.55/0.46
Q[f], $\lvert e\rvert \times 10^{-24}$ cm^2	−0.789	0.293/0.27	−0.08/−0.06

[a] The order of the components of the **A** and **P** matrices is given with respect to the **g** components g_{max}, g_{mid}, and g_{min}. [b] The **A**-tensor components, of which the first two oriented along g_{max} and g_{mid} are upper limits estimated from the envelope of the respective line. The signs are arbitrary; they cannot be determined from simulations. [c] Quadrupole coupling matrix; the sign of the main component is again arbitrary. [d] Euler angle that rotates the respective **P** matrix around the direction of g_{mid}. [e] Nuclear g factor. [f] Quadrupole moment.

$[Fe^{II}('N_2S_2^{\bullet\bullet\prime})(PPh_3)]$ and $[Fe^{III}('N_2S_2^{\bullet\bullet})I]$ have been reported previously.[6,7]

In part 1[8] of the present series, we have described the structure of **5a**·$2CH_3CN$·CH_2Cl_2, which contains two intermediate-spin ferric ions, two terminal N,S-coordinated *o*-aminothiophenolato-(1−), $(L^{AP})^-$, ligands, and two bridging *o*-iminothiophenolato-(2−), $(L^{IP})^{2-}$, ligands. The imino nitrogens of the latter ligands are the bridging atoms. The oxidation level of the ligands is clearly established by the fact that the C−S distances are long at ∼1.77 Å, and the six-membered phenyl rings display, within an experimental error of $3\sigma = \pm 0.01$ Å, six nearly equivalent C−C bonds at 1.40 ± 0.01 Å. It is now interesting to compare the structure of **5a** with that of **7** shown in Figure 7, where the dimer formation is also accomplished by two μ-imino nitrogens. Thus, **5a** and **7** possess the same FeN_3S_2 square-based pyramidal polyhedra. It is immediately evident that **7** has two protons per dimer less than **5a**: all four nitrogen atoms are imino nitrogens in **7**. The most striking geometrical features are the observations that (1) both *terminally* N,S-coordinated ligands are unequivocally *o*-iminothionebenzosemiquinonate(1−) π radicals, $(L^{ISQ})^-$, because their C−S bonds are short at 1.74 ± 0.01 as are the C−N bonds at 1.39 Å and the phenyl ring clearly shows the quinoid-type distortions typical for semiquinonates and that (2) both *bridging* N,S-coordinated ligands are of the *o*-iminothiophenolato(2−) type, $(L^{IP})^{2-}$, because the C−S and C−N bonds at 1.765 and 1.422 Å, respectively, are long and the six C−C bonds are equivalent (av ∼1.40 ± 0.01 Å). Thus, in **7** an oxidation level of $[Fe^{III}(L^{IP})(L^{ISQ})]_2$ is prevalent. This is also corroborated by the fact that the sum of the five Fe−X bonds in **5a** at 10.477 Å and in **7** at 10.328 Å are very similar, indicating similar spin states of the iron ions in both complexes.

Similarly, the structure of **6** shown in Figure 8 immediately reveals that the oxidation level is again $[Fe^{III}(L^{IP})(L^{ISQ})]_2$, the same as that in **7**. Two terminal N,S-coordinated $(L^{ISQ})^-$ π radicals and two bridging $(L^{IP})^{2-}$ closed-shell ligands are clearly present. Thus, **6** and **7** are geometrical isomers, where the didentate $(L^{IP})^{2-}$ and $(L^{ISQ})^-$ ligands of half of a dimer are in the trans position relative to each other, whereas in **7** they are in the cis position. Compound **6** is (μ-NH,NH)-bridged, whereas complex **7** is (μ-S,S)-bridged. Previously, we structurally characterized the cobalt complex $(\mu\text{-S,S})[Co^{II}(L^{ISQ})_2]_2$.[14] Figure

(14) Herebian, D.; Ghosh, P.; Chun, H.; Bothe, E.; Weyhermüller, T.; Wieghardt, K. *Eur. J. Inorg. Chem.* **2002**, 1957.

Table 4. Bond Distances (Å) in Complexes **6**−**9**

				Complex **6**					
Fe1−N2	1.851(6)	Fe1−Fe1*	2.816(2)	C2−C3	1.391(10)	S2−C21	1.727(7)	C22−C23	1.414(9)
Fe1−N1	1.872(6)	S1−C1	1.780(7)	C3−C4	1.372(10)	N2−C22	1.360(9)	C23−C24	1.377(10)
Fe1−S2	2.187(2)	N1−C2	1.373(9)	C4−C5	1.423(11)	C21−C22	1.412(10)	C24−C25	1.420(10)
Fe1−S1	2.227(2)	C1−C2	1.408(10)	C5−C6	1.392(10)	C21−C26	1.426(10)	C25−C26	1.352(10)
Fe1−S1*	2.347(2)	C1−C6	1.426(10)						
				Complex **7**					
Fe1−N1	1.919(3)	Fe1−Fe1*	2.664(1)	C1−C2	1.420(4)	C4−C5	1.421(4)	C22−C23	1.397(4)
Fe1−N2	1.924(3)	S1−C1	1.742(3)	C1−C6	1.429(5)	C5−C6	1.383(5)	C23−C24	1.384(5)
Fe1−N2*	2.080(3)	S2−C21	1.765(3)	C2−C3	1.400(5)	C21−C22	1.398(4)	C24−C25	1.397(4)
Fe1−S1	2.196(1)	N1−C2	1.386(4)	C3−C4	1.374(5)	C21−C26	1.423(5)	C25−C26	1.391(4)
Fe1−S2	2.209(1)	N2−C22	1.422(4)						
				Complex **8**					
Fe(1)−N(10)	1.882(7)	C(15)−C(16)	1.353(13)	Fe(4)−S(41)	2.322(3)	N(67)−C(68)	1.432(11)	N(87)−C(88)	1.443(12)
Fe(1)−N(7)	1.890(7)	S(21)−C(21)	1.785(9)	S(41)−C(41)	1.750(9)	C(68)−C(69)	1.496(12)	C(88)−C(89)	1.496(13)
Fe(1)−S(12)	2.207(3)	S(32)−C(32)	1.735(10)	S(52)−C(52)	1.720(10)	C(69)−N(70)	1.446(11)	C(89)−N(90)	1.427(11)
Fe(1)−S(1)	2.229(3)	C(21)−C(22)	1.379(12)	C(41)−C(42)	1.387(13)	N(70)−C(71)	1.370(11)	N(90)−C(91)	1.362(11)
Fe(1)−S(21)	2.349(3)	C(21)−C(26)	1.389(12)	C(41)−C(46)	1.406(12)	C(71)−C(72)	1.406(12)	C(91)−C(92)	1.411(13)
Fe(1)−Fe(2)	2.876(2)	C(22)−C(23)	1.380(13)	C(41)−C(46)	1.406(12)	C(71)−C(76)	1.429(12)	C(91)−C(96)	1.445(13)
Fe(2)−N(30)	1.872(7)	C(23)−C(24)	1.378(14)	C(42)−C(43)	1.404(13)	C(72)−C(73)	1.410(12)	C(92)−C(93)	1.405(13)
Fe(2)−N(27)	1.887(7)	C(24)−C(25)	1.357(13)	C(43)−C(44)	1.373(14)	C(73)−C(74)	1.370(13)	C(93)−C(94)	1.380(14)
Fe(2)−S(32)	2.213(3)	C(25)−C(26)	1.393(12)	C(44)−C(45)	1.387(14)	C(74)−C(75)	1.416(14)	C(94)−C(95)	1.39(2)
Fe(2)−S(21)	2.228(3)	C(26)−N(27)	1.375(11)	C(45)−C(46)	1.406(13)	C(75)−C(76)	1.365(12)	C(95)−C(96)	1.359(15)
Fe(2)−S(1)	2.343(3)	N(27)−C(28)	1.389(11)	C(46)−N(47)	1.368(11)	Fe(5)−N(90)	1.863(7)	S(101−C(101)	1.767(9)
S(1)−C(1)	1.771(9)	C(28)−C(29)	1.467(12)	N(47)−C(48)	1.444(11)	Fe(5)−N(87)	1.869(8)	S(112)−C(112)	1.721(9)
S(1)−C(1)	1.771(9)	C(29)−N(30)	1.411(11)	C(48)−C(49)	1.485(13)	Fe(5)−S(92)	2.202(3)	C(101)−C(102)	1.380(12)
S(12)−C(12)	1.723(10)	N(30)−C(31)	1.358(11)	C(49)−N(50)	1.442(11)	Fe(5)−S(81)	2.216(3)	C(101)−C(106)	1.413(13)
C(1)−C(2)	1.385(12)	C(31)−C(36)	1.416(12)	N(50)−C(51)	1.368(11)	Fe(5)−S(101)	2.336(3)	C(102)−C(103)	1.406(14)
C(1)−C(6)	1.413(12)	C(31)−C(32)	1.436(13)	C(51)−C(56)	1.413(13)	Fe(5)−Fe(6)	2.796(2)	C(103)−C(104)	1.374(15)
C(2)−C(3)	1.392(13)	C(32)−C(33)	1.384(12)	C(51)−C(52)	1.414(12)	Fe(6)−N(110)	1.858(7)	C(104)−C(105)	1.374(13)
C(3)−C(4)	1.379(13)	C(33)−C(34)	1.387(13)	C(52)−C(53)	1.407(13)	Fe(6)−N(107)	1.874(7)	C(105)−C(106)	1.402(12)
C(4)−C(5)	1.367(13)	C(34)−C(35)	1.369(14)	C(53)−C(54)	1.390(14)	Fe(6)−S(112)	2.199(3)	C(106)−N(107)	1.367(11)
C(5)−C(6)	1.400(12)	C(35)−C(36)	1.378(13)	C(54)−C(55)	1.365(14)	Fe(6)−S(101)	2.221(3)	N(107)−C(108)	1.445(11)
C(6)−N(7)	1.379(11)	Fe(3)−N(50)	1.859(7)	C(55)−C(56)	1.365(14)	Fe(6)−S(81)	2.332(3)	C(108)−C(109)	1.479(12)
N(7)−C(8)	1.417(11)	Fe(3)−N(47)	1.873(7)	S(61)−C(61)	1.757(9)	S(81)−C(81)	1.786(10)	C(109)−N(110)	1.463(11)
C(8)−C(9)	1.473(13)	Fe(3)−S(52)	2.204(3)	S(72)−C(72)	1.740(9)	S(92)−C(92)	1.728(10)	N(110)−C(111)	1.377(11)
C(9)−N(10)	1.408(11)	Fe(3)−S(41)	2.220(3)	C(61)−C(62)	1.399(12)	C(81)−C(82)	1.371(14)	C(111)−C(112)	1.412(12)
N(10)−C(11)	1.388(11)	Fe(3)−S(61)	2.361(3)	C(61)−C(66)	1.406(12)	C(81)−C(86)	1.407(14)	C(111)−C(116)	1.423(12)
C(11)−C(12)	1.400(13)	Fe(3)−Fe(4)	2.831(2)	C(62)−C(63)	1.369(13)	C(82)−C(83)	1.41(2)	C(112)−C(113)	1.384(12)
C(11)−C(16)	1.408(13)	Fe(4)−N(70)	1.870(7)	C(63)−C(64)	1.366(14)	C(83)−C(84)	1.37(2)	C(113)−C(114)	1.389(13)
C(12)−C(13)	1.411(13)	Fe(4)−N(67)	1.882(7)	C(64)−C(65)	1.382(13)	C(84)−C(85)	1.36(2)	C(114)−C(115)	1.376(13)
C(13)−C(14)	1.370(14)	Fe(4)−S(72)	2.208(3)	C(65)−C(66)	1.406(12)	C(85)−C(86)	1.425(14)	C(115)−C(116)	1.366(13)
C(14)−C(15)	1.389(14)	Fe(4)−S(61)	2.226(3)	C(66)−C(67)	1.372(11)	C(86)−C(87)	1.366(12)		
				Complex **9**					
Fe1−N2	1.848(2)	S1−C1	1.733(3)	C1−C6	1.420(4)	C2−C3	1.416(4)	C4−C5	1.423(4)
Fe1−P1	2.149(2)	N2−C2	1.352(3)	C1−C2	1.430(4)	C3−C4	1.366(4)	C5−C6	1.378(4)
Fe1−S1	2.191(1)								

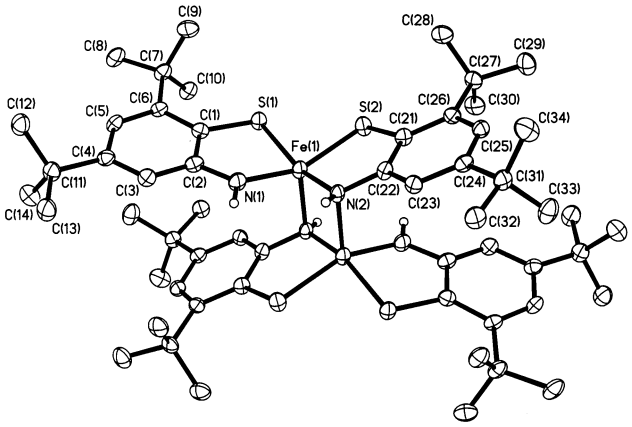

Figure 7. Structure of the neutral (μ-NH,NH)-bridged dimer in crystals of **7**. The small open circles represent located imino hydrogen atoms; all other hydrogens are omitted.

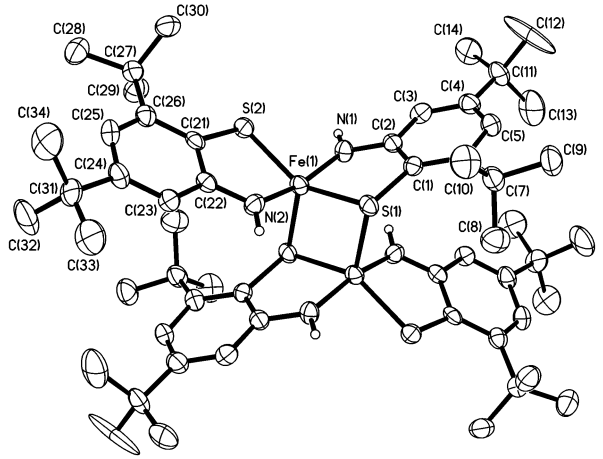

Figure 8. Structure of the neutral (μ-S,S)-bridged dimer in crystals of **6**.

9 shows the bond distances in this compound and in **6**. Clearly, the bond distances of the *terminal* π radicals in both compounds are identical within an experimental error of ± 0.01 Å, but those of the *bridging* ligands are not; they are typical for a π radical in the cobalt compound but closed-shell aromatic, $(L^{IP})^{2-}$, in the iron species **6**. This demonstrates that high-quality, low-

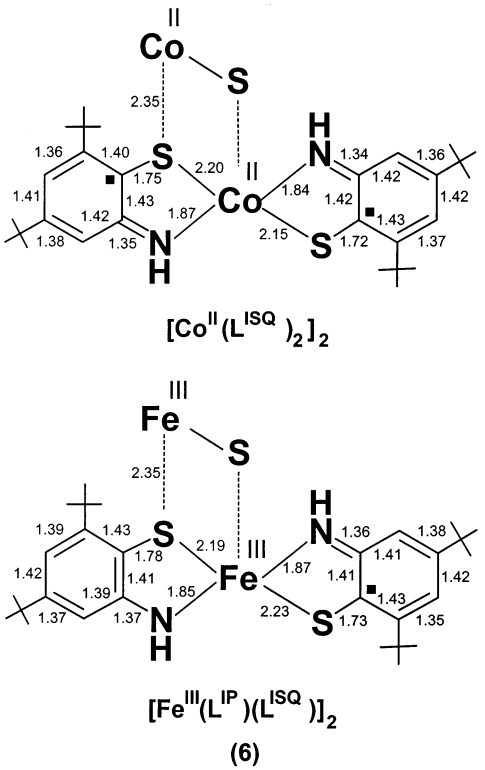

Figure 9. Comparison of bond distances (Å) in (μ-S,S)[$Co^{II}(L^{ISQ})_2$]$_2$ (top) from ref 14 and **6** (bottom).

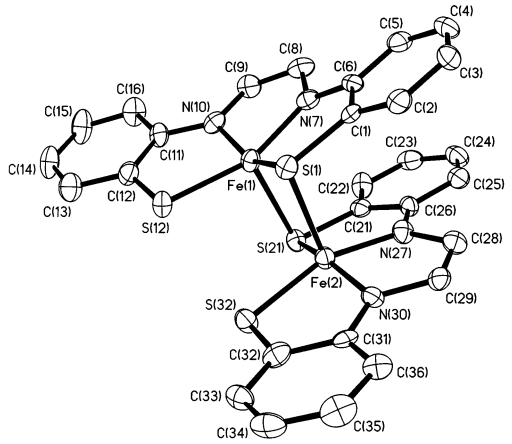

Figure 10. One of the three crystallographically independent dimers in crystals of **8**.

temperature X-ray crystallography is a very powerful tool in establishing the oxidation level of a given ligand in such complexes. Note that the cobalt species furnishes the first structurally characterized example of a bridging $(L^{ISQ})^-$ radical.

Crystals of **8** contain three crystallographically independent dimers, one of which is shown in Figure 10. In each of these three cases, the terminally N,S-coordinated half of the $'N_2S_2'$ ligand is an *o*-iminothionesemiquinonate(1−) radical, as was judged from their uniformly short C−S distances (av 1.728 Å) and the quinoid-type distortion of the corresponding six-membered rings. For the bridging part, the C−S distances are long (av 1.77 Å) and indicate the presence of an *o*-iminothiophenolato(2−) oxidation level. This renders the central metal ion a ferric ion. The structures of the three dimers vary slightly, as is judged by their significantly differing Fe···Fe′ distances of 2.876(2), 2.831(2), and 2.796(2) Å, but there is no structural indication for a (μ-S,S)[$Fe^{II}('N_2S_2^{\bullet\bullet\prime})$]$_2$ oxidation-state distribution.

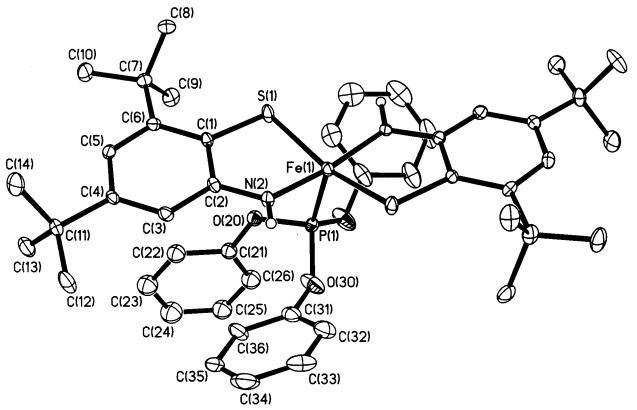

Figure 11. Structure of a neutral monomer in crystals of **9**. The small open circles represent located imino hydrogen atoms; all other hydrogens are omitted.

Figure 11 exhibits the structure of the neutral molecule in crystals of **9**. The two N,S-coordinated *o*-iminothionebenzosemiquinonato(1−) radicals are in the trans position relative to each other; the C−S bond at 1.733(3) Å is short, and the six-membered ring clearly shows the quinoid-type distortions. [$Fe^{II}('N_2S_2^{\bullet\bullet})(P(i\text{-}Pr)_3)$] and [$Fe^{II}('N_2S_2^{\bullet\bullet})(PPh_3)$] have been structurally characterized previously.[6] The geometrical features of the $('N_2S_2^{\bullet\bullet\prime})^{2-}$ ligands are very similar to those reported here for **9** and indicate their semiquinonate character.[1] This renders the iron ions divalent. The Fe−N and Fe−S bond lengths at 1.848(2) and 2.191(1) Å are short and rule out a high-spin ferrous configuration as in **2** or **3**, where these distances are found at >2.1 and >2.3 Å, respectively.[8] Thus, the present structure supports a low-spin ferrous configuration in **9** that is stabilized by the very strong phosphine or phosphite σ donor.

As we have pointed out previously,[2] the crystal structure of [$Fe^{III}('N_2S_2^{\bullet\bullet})$I], which shows spectroscopically nearly the same features as complexes **11a**−**c**, clearly indicates that both halves of the ligand $('N_2S_2^{\bullet\bullet\prime})^{2-}$ are of the *o*-iminothionebenzosemiquinonate(1−) π radical type: the C−S bonds at 1.72 Å are short, and the six-membered rings show quinoid-type distortions. This renders the central iron ion ferric.

Mössbauer Spectroscopy. Zero-field Mössbauer spectra of the polycrystalline samples were recorded at 80 K; the results are summarized in Table 5. The spectra of **6**, **7**, **11a**−**c**, and [$Fe^{III}('N_2S_2^{\bullet\bullet\prime})$I][7] consist of a single doublet with very similar isomer shift, δ, and quadrupole splitting, ΔE_Q, parameters: $\delta = 0.15-0.33$ mm s^{-1} and $\Delta E_Q = 2.06-3.4$ mm s^{-1}. The zero-field spectrum at 80 K of **8** exhibits a very broad doublet, which from applied field spectra at 4.2 K can be deconvoluted into two subspectra (48:52): for 1, $\delta = 0.16$ mm s^{-1}, $\Delta E_Q = 2.68$ mm s^{-1}, and $\eta = 0.43$ and for 2, $\delta = 0.25$ mm s^{-1}, $\Delta E_Q = 2.06$ mm s^{-1}, $\eta = 0.43$. This is shown in Figure 12. Both parameter sets are similar to those observed for **6** and **7**, and the spin state of the iron ions is the same. This is independent of the overall ground state, S_t, of the complexes. It indicates a common local spin state of the respective iron ion of $S_{Fe} = {}^3/_2$. The data are also very similar to those of **5a** and **5b** and a number of the five-coordinate complexes containing genuine intermediate-spin iron ions as compiled in part 1 of the present series.[15−18] The magnetically perturbed Mössbauer spectra of

Table 5. Zero-Field Mössbauer Parameters of Complexes

complex	T, K	δ^a, mm s^{-1}	$\lvert\Delta E_Q\rvert^b$, mm s^{-1}	$S_{Fe}{}^c$	$S_t{}^d$
2	80	0.85	3.68	2	0
3	80	0.87	3.24	2	0
5a	80	0.33	0.93	$^3/_2$	0
5b	80	0.30	2.71	$^3/_2$	0
6	80	0.17	2.73	$^3/_2$	0
7	80	0.20	2.67	$^3/_2$	0
8	80	0.16	2.68	$^3/_2$	0
		0.25	2.06	$^3/_2$	0
9	80	0.06	2.92	0	0
10	80	0.05	2.98	0	0
11a	80	0.15	3.09	$^3/_2$	$^1/_2$
11b	80	0.15	3.07	$^3/_2$	$^1/_2$
11c	80	0.17	2.97	$^3/_2$	$^1/_2$
[Fe^{II}('N$_2$S$_2^{\bullet\bullet\prime}$)(PPh$_3$)]^e	4.2	0.04	3.16	0	0
[Fe^{III}('N$_2$S$_2^{\bullet\bullet\prime}$)I]^f	4.2	0.11	3.41	$^3/_2$	$^1/_2$

^{a} Isomer shift versus αFe at 289 K. ^{b} Quadrupole splitting. ^{c} Local spin state at the iron ion. ^{d} Ground state. ^{e} Reference 6. ^{f} Reference 7.

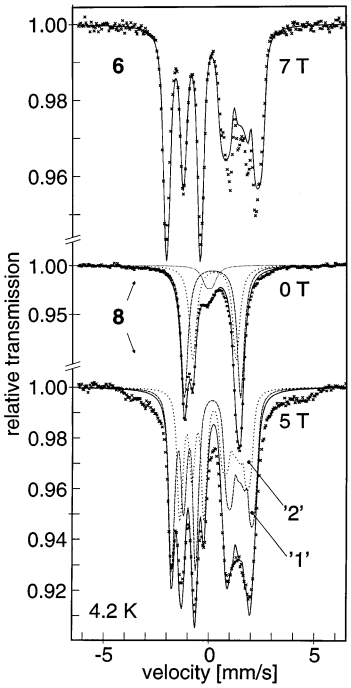

Figure 12. Magnetic Mössbauer spectra of solid **6** and **8** at 4.2 K and 7-, 5-, and 0-T field applied perpendicular to the γ rays. The lines are nuclear simulations ($S = 0$) with the following parameters: $\delta = 0.17$ mm s^{-1}, $\Delta E_Q = 2.70$ mm s^{-1}, $\eta = 0.42$ (**6**); $\delta = 0.16$ mm s^{-1}, $\Delta E_Q = 2.68$ mm s^{-1}, $\eta = 0.43$ (**8**, subspectrum 1); $\delta = 0.25$ mm s^{-1}, $\Delta E_Q = 2.06$ mm s^{-1}, $\eta = 0.43$ (**8**, subspectrum 2).

6 and **8** shown in Figure 12 support the observed $S_t = 0$ ground state. For **6**, the following parameters were obtained at 4.2 K: $\delta = 0.17$ mm s^{-1}, $\Delta E_Q = 2.70$ mm s^{-1}, and $\eta = 0.42$.

The zero-field spectra of complexes **9**, **10**, and [Fe^{II}('N$_2$S$_2^{\bullet\bullet\prime}$)(PR$_3$)] also consist of a single quadrupole doublet with a rather small isomer shift of 0.04−0.06 mm s^{-1} and a large quadrupole splitting of 2.92−3.16 mm s^{-1}. These data point to the presence of a five-coordinate low-spin ferrous ion (d,[6] $S_{Fe} = 0$) in these complexes. Applied-field Mössbauer measurements support the

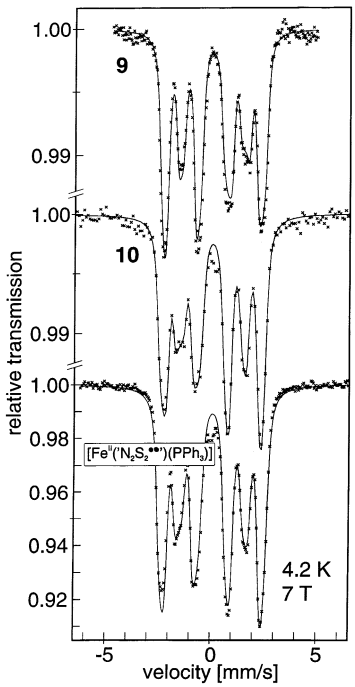

Figure 13. Magnetic Mössbauer spectra of solid **9**, **10**, and [Fe^{II}('N$_2$S$_2^{\bullet\bullet\prime}$)-(PPh$_3$)$_2$] at 4.2 K and 7-T field applied perpendicular to the γ rays. The lines are nuclear simulations ($S = 0$) with the following parameters: $\delta = 0.06$ mm s^{-1}, $\Delta E_Q = 2.95$ mm s^{-1}, $\eta = 0.77$ (**9**); $\delta = 0.05$ mm s^{-1}, $\Delta E_Q = -2.97$ mm s^{-1}, $\eta = 0.71$ (**10**); $\delta = 0.07$ mm s^{-1}, $\Delta E_Q = -3.06$ mm s^{-1}, $\eta = 0.88$ {[Fe^{II}('N$_2$S$_2^{\bullet\bullet\prime}$)(PPh$_3$)$_2$]}.

observation of diamagnetic ground states for **9**, **10**, and [Fe^{II}-('N$_2$S$_2^{\bullet\bullet\prime}$)(PPh$_3$)]. The magnetic splittings of the spectra measured at 4.2 K and shown in Figure 13 are diamagnetic patterns resulting from the nuclear Zeeman splittings induced by a strong external magnetic field of 7 T, the simulations of which corroborate the complete absence of internal fields. The high-oxidation-state Fe(IV) with $S = 1$, as implied in the original publication[6] for [Fe('N$_2$S$_2^{\bullet\bullet\prime}$)(PR$_3$)], is not corroborated by our data on the same compounds. The 7-T Mössbauer spectrum of [Fe^{II}('N$_2$S$_2^{\bullet\bullet\prime}$)(PPh$_3$)] was readily fitted assuming an $S_t = 0$ ground state (Figure 13). Therefore, our observation of an $S_t = 0$ ground state for [Fe^{II}('N$_2$S$_2^{\bullet\bullet\prime}$)(PPh$_3$)] makes our previous analyses of the original Mössbauer spectra in ref 1 assuming an $S_t = 1$ ground state obsolete. Large quadrupole splittings are not without precedent for five-coordinate square-base pyramidal low-spin ferrous complexes with covalently bound axial ligands. Although the 3d(t_{2g})^6 configuration has no valence contribution to the EFG, strong covalency from the axial ligand can induce significant charge asymmetries and strong EFGs at the iron nucleus. The asymmetry parameters, η, of **9**, **10**, and [Fe('N$_2$S$_2^{\bullet\bullet\prime}$)(PPh$_3$)] are large and close to the limit of 1. Consequently, the signs of the EFG main components are without significant physical meaning.

Mössbauer spectra with applied fields of 1−7 T of **11a**−**c** were measured at 4.2 K to determine the intrinsic spin state of iron and the spin-coupling schemes of the radical complexes. For solid samples, however, diamagnetic spectra were obtained with only weak magnetic splittings, which in the cases of **11b** and **11c** can be readily simulated by the effect of the applied fields only (Figure 14). This behavior is not unexpected because of the intramolecular antiferromagnetic interactions observed from the susceptibility measurements.

(15) Sawyer, D. T.; Srivatsa, G. S.; Bodini, M. E.; Schaefer, W. P.; Wing, R. M. *J. Am. Chem. Soc.* **1986**, *108*, 936.
(16) Niarchos, D.; Kostikas, A.; Simopoulos, A.; Coucouvanis, D.; Piltingsrud, D.; Coffman, R. E. *J. Chem. Phys.* **1978**, *69*, 4411.
(17) Keutel, H.; Käpplinger, I.; Jäger, E.-G.; Grodzicki, M.; Schünemann, V.; Trautwein, A. X. *Inorg. Chem.* **1999**, *38*, 2320.
(18) Kostka, K. L.; Fox, B. G.; Hendrich, M. P.; Collins, T. J.; Rickard, C. E. F.; Wright, L. J.; Münck, E. *J. Am. Chem. Soc.* **1993**, *115*, 6746.

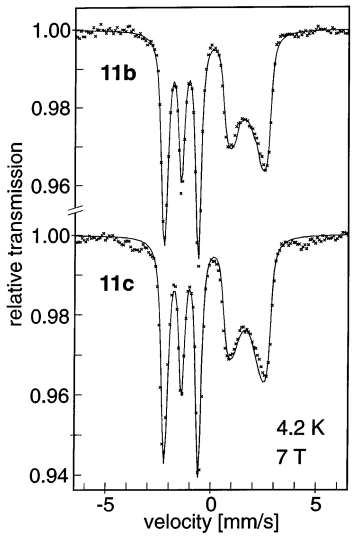

Figure 14. Magnetic Mössbauer spectra of solid **11a** and **11b** measured at 4.2 K and 7-T field applied perpendicular to the γ rays. The solid line is a simulation including nuclear Zeeman and quadrupole interactions and electronic spin $S = 0$. Parameters: $\delta = 0.16$ mm s^{-1}, $\Delta E_Q = 3.09$ mm s^{-1}, $\eta = 0.17$ (**11b**); $\delta = 0.17$ mm s^{-1}, $\Delta E_Q = 2.96$ mm s^{-1}, $\eta = 0.37$ (**11c**).

The cancellation of internal fields is not complete for solid compound **11a** because of weaker intermolecular interactions. The presence of a weak spin-expectation value is shown in Figure 15, right column. The theoretical spectrum for $S = 0$, which is overlayed as a thin dotted line to the 7-T spectrum (right, bottom), has a *wider* magnetic splitting than that of the experimental spectrum. The magnetic spectra of solid **11a** can be well-simulated in the entire field range by using the dimer approach of interacting molecule pairs introduced above. The simulations yield a sizable hyperfine coupling tensor of $\mathbf{A}/g_N\beta_N(S_t = {}^1/_2) = (-12.31, -26.75, +1.0)$ T with respect to the "local" molecule spin $S_t = {}^1/_2$. The presence of a strong intrinsic spin density at the iron site of **11a** was nicely corroborated by measurements on a frozen acetonitrile *solution* (1 mM, 35% ^{57}Fe), which show much larger magnetic splittings due to the presence of *monomeric* molecules with strong internal fields that are not attenuated by intermolecular coupling. The spectra could be deconvoluted by a superposition of 65% **11a** *monomers* and 35% persisting *dimers*, similar to those prevailing in the solid. A consistent simulation of the solid and solution data together was obtained with the hyperfine coupling tensors $\mathbf{A}/g_N\beta_N(S_t = {}^1/_2) = (-12.31, -26.75, +1.0)$ T, which was kept identical for both the solution species and solid. The intermolecular coupling constants are found to be $J_m = -3.6$ cm^{-1} for the fictitious dimers with $S_{t,1} = {}^1/_2$ and $S_{t,2} = {}^1/_2$ in the solid (fast-spin relaxation limit) and $J_m = -2.96$ cm^{-1} in the solution (slow-spin relaxation). Interestingly, the minute differences in J_m are technically significant for the Mössbauer simulations at the given conditions of magnetic and electric hyperfine interactions.

Electronic Structure of 11a−c. The total spin ground state $S_t = {}^1/_2$ of compounds **11a−c** is, in principle, consistent with three different interpretations of the electronic structure of the complexes: it might owe its origin either to the presence of a low-spin ($S_{Fe} = {}^1/_2$) iron(III) ion that is antiparallelly spin-aligned to the radical spins (in the linear arrangement labeled as [↑↓↑]), to a low-spin iron(III) ion and antiparallelly aligned radical spins ([↑↑↓]), or to an iron(III) ion of *intermediate*-spin

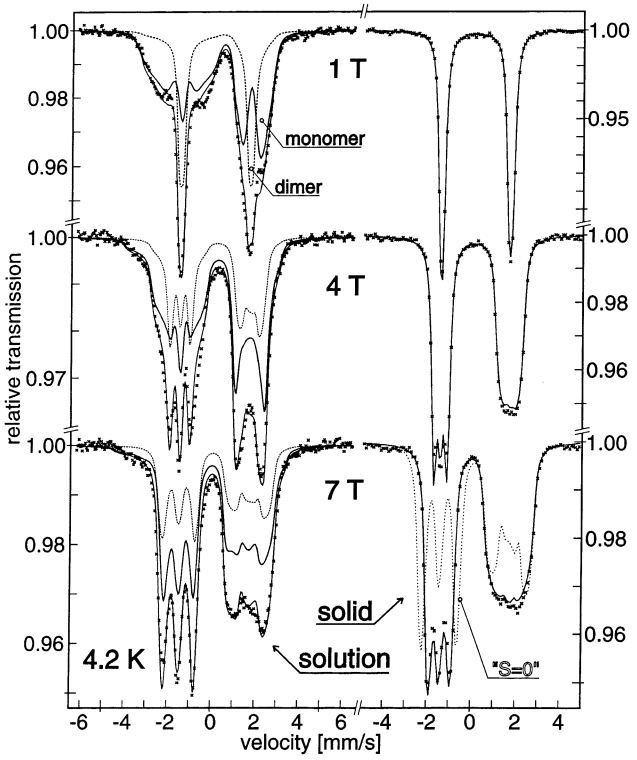

Figure 15. Magnetic Mössbauer spectra of **11a** in the solid (right) and frozen (left) forms at 4.2 K and fields of 1, 4, and 7 T applied perpendicular to the γ rays. The lines are spin Hamiltonian simulations described in the text. Parameters: $\delta = 0.15$ mm s^{-1}, $\Delta E_Q = 3.11$ mm s^{-1}, $\eta = 0.4$, $J_m = -3.6$ cm^{-1} (*solid*, fast relaxation); $\delta = 0.12$ mm s^{-1}, $\Delta E_Q = +3.18$ mm s^{-1}, $\eta = 0.53$ (*solution monomers*, left solid line, slow relaxation); $\delta = 0.12$ mm s^{-1}, $\Delta E_Q = +3.18$ mm s^{-1}, $\eta = 0.53$, $J_m = -2.96$ cm^{-1} (*solution dimers*, left dashed line, slow relaxation). The same **g** values and **A** tensors were used throughout: $\mathbf{g} = (2.26, 2.03, 2.12)$, $\mathbf{A}/g_N\beta_N(S_t = {}^1/_2) = (-12.31, -26.75, +1.0)$ T.

($S_{Fe} = {}^3/_2$) that is coupled in an antiparallel fashion to the ligand radicals ([↓↑↓]). Because the molecular structures of compounds **11a−c** presumably involve five-coordinated iron sites and because square-pyramidal ligand fields often induce an *intermediate* spin state, the latter case should prevail for these compounds.

This presumption can be experimentally established for **11a** from an interpretation of the EPR **g** values, the Mössbauer magnetic hyperfine coupling tensor **A**, and the EFG at the ^{57}Fe nucleus. When the measured **A**-tensor components $A_i(S_t = {}^1/_2)$ (Figure 15) are converted to intrinsic values for $S_{Fe} = {}^3/_2$ by using the relation $A_i(S_{Fe} = {}^3/_2) = {}^3/_5 A_i(S_t = {}^1/_2)$ derived from spin-projection techniques, one obtains $\mathbf{A}(S_{Fe} = {}^3/_2)/g_N\beta_N = (-7.38, -16.05, +0.60)$ T with an isotropic part $A_{iso}(S_{Fe} = {}^3/_2)/g_N\beta_N = -7.62$ T. Although the values are quite small compared to typical high-spin data (≈ -20 T), they closely resemble the tensors $\mathbf{A}/g_N\beta_N = (-12.7, -12.7, +0.50)$ T and $\mathbf{A}/g_N\beta_N = (-22, -16.6, +5)$ T reported for the well-characterized monomeric *intermediate*-spin iron(III) complexes LFeI and L′FeCl of Jäger et al.[17] and Collins et al.,[18] where L and L′ are innocent N-donor macrocycles. In particular, the similarity of the pronounced **A** anisotropies with the unusual positive *z* components is significant and is also found in other well-studied examples.[16,19] Large quadrupole splittings of more than +3 mm s^{-1} and a positive EFG main component V_{zz} along the minor component of the **A** tensor, as is observed for **11a**, were

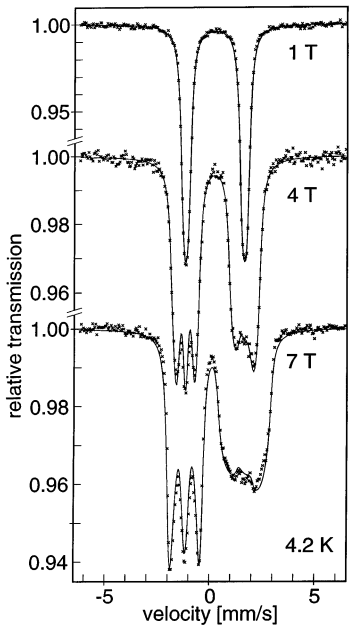

Figure 16. Magnetic Mössbauer spectra of solid $[Fe^{III}(L^{ISQ}{}_o)_2I]$ at 4.2 K and fields of 1, 4, and 7 T applied perpendicular to the γ rays. The lines are spin Hamiltonian simulations ($S = {}^1/_2$) with the following parameters: $\delta = 0.24$ mm s^{-1}, $\Delta E_Q = +2.80$ mm s^{-1}, $\eta = 0.25$, $\mathbf{g} = (2.19, 2.19, 2.13)$, $\mathbf{A}/g_N\beta_N(S_t = {}^1/_2) = (-20.67, -33.89, +2.16)$ T (fast relaxation).

recognized early as additional characteristic features of intermediate-spin iron(III).[20] Grodzicki et al. provided an elaborate molecular orbital interpretation of these spectroscopic properties for LFeI,[17] which traces the origin of the EFG back to a covalent population of the otherwise unpopulated $x^2 - y^2$ orbital. This treatment resolves the problem that in a basic ligand-field picture the $3d_{xy}{}^2 3d_{xz}{}^1 3d_{yz}{}^1 3d_{z^2}{}^1 3d_{x^2-y^2}{}^0$ configuration that results from destabilization of the $x^2 - y^2$ orbital by the dominating strong antibonding interaction with the equatorial ligands would predict a vanishing EFG, $\Delta E_Q \approx 0$, in crude contrast to experiment. Also, the unusually low isomer shift of the radical complexes **11a**−**c** (0.15−0.17 mm s^{-1}) is consistent with that of the intermediate-spin compound LFeI ($\delta = 0.18$ mm s^{-1});[17] a somewhat higher value is reported for L′FeCl (0.25 mm s^{-1}).[18] The latter value is close to the isomer shift of the structurally characterized *o*-iminobenzosemiquinonato complex $[Fe^{III}(L_o{}^{ISQ})_2I]$ that we reported previously[2] and has a N_2O_2I Fe coordination polyhedron. The presence of intermediate-spin iron(III) in this example and the related halido analogues was inferred from magnetic-susceptibility measurements because the exchange coupling of iron and radicals is less than that for the *o*-iminothiobenzosemiquinonato complexes presented here, and excited spin states above the $S_t = {}^1/_2$ ground state are populated and detectable at ambient temperature.

For comparison and completeness, we also measured and analyzed the magnetic Mössbauer spectra of solid $[Fe^{III}(L_o{}^{ISQ})_2I]$ because this compound did not show sizable intermolecular interactions (Figure 16). The simulations reveal close similarity of $[Fe^{III}(L_o{}^{ISQ})_2I]$ and **11a**−**c**, with the characteristic difference that the **A**-tensor components $\mathbf{A}/g_N\beta_N(S_t = {}^1/_2) = (-20.67, -33.89, +2.16)$ T are larger than those of **11a**. The difference, as well as the larger isomer shift, can be explained by the reduced covalency of the N_2O_2I coordination sphere with respect to that of the N_2S_2X ligands of **11a**−**c**. The intrinsic **A** values $\mathbf{A}(S_{Fe} = {}^3/_2)/g_N\beta_N = (-12.4, -20.3, +1.3)$ T of iron(III) fit nicely to those of Collins et al.'s L′FeCl compound[18] $[\mathbf{A}/g_N\beta_N = (-16.6, -22, +5)$ T]. Thus, the spectroscopic properties of the $[Fe^{III}(L^{ISQ})_2X]$ complexes are readily consistent with the presence of intermediate-spin iron(III).

The possible alternative low-spin configuration of iron(III) can be ruled out from two further considerations of the magnetic properties of **11a**: the spin-coupling scheme of antiferromagnetic alignment of low-spin iron(III) and the radicals (case [↑↓↑] from above) is excluded because the antiparallel orientation of the *iron* spin and *total* spin would induce a *positive* trace of the measurable **A** tensor for the ground state $S_t = {}^1/_2$, in contrast to the data obtained for **11a**. In the second case, [↑↑↓], antiparallel orientation of the radical spins would virtually cancel the influence of the radicals so that the spectroscopic properties would be exclusively determined by the central ferric ion.[21] However, when the electronic **g**-tensor value taken from the EPR spectra (2.12, 2.03, 2.26) is used to derive a description of the spin−orbit interaction and orbital mixing of the $(t_{2g})^5$ configuration in a crystal-field model,[22] the best approach for low-spin iron(III) in **11a** would be characterized by large axial and rhombic orbital splittings that render the electron hole predominantly in an *xz* or *yz* orbital.[23] The EFG resulting from the corresponding charge distribution would exhibit a *negative* main component of about −1.5 mm s^{-1}, and the magnetic hyperfine tensor would be expected to show a single, large main component in the direction of the EFG main component.[24] Because both features, the sign of the predicted EFG main component and the symmetry of the **A** tensor (two large components, one minor), are in gross contrast to experiment, we can exclude the presence of low-spin iron(III).

The model of intermediate-spin iron(III) compounds with ligand radicals also provides a plausible interpretation of the remarkable quadrupole effect of the EPR spectra of **11a** and **11b** described above. It arises from the strong EFG at the halide *ligand* nuclei with the main component oriented *perpendicular* to the main **A**-tensor component. The major contribution to the EFG at iodine and bromine should result from the anisotropic delocalization of the p_x, p_y, and p_z orbitals by different covalent interactions with the corresponding iron d orbitals and the resulting *charge anisotropy* of the ligand p shell. For the apical ligand, p_z should be distinctly more delocalized by σ interaction with d_{z^2} than p_x and p_y by π interaction with d_{xz} and d_{yz},

(19) (a) Ganguli, P.; Marathe, V. R.; Mitra, S. *Inorg. Chem.* **1975**, *14*, 970. (b) Wells, F. V.; McCann, S. W.; Wickman, H. H.; Kessel, S. L.; Hendrickson, D. N.; Feltham, R. D. *Inorg. Chem.* **1982**, *21*, 2306.

(20) (a) Dolphin, D. H.; Sams, J. R.; Tsin, T. B. *Inorg. Chem.* **1977**, *16*, 711. (b) Maltempo, M. M. *J. Chem. Phys.* **1974**, *61*, 2540. (c) Maltempo, M. M.; Moss, T. H. *Q. Rev. Biophys.* **1976**, *9*, 181.

(21) Mixing of the two ground-state and excited-state spin doublets that result from the spin coupling of three local spin doublets is assumed to be vanishing because of the unmeasurable large exchange splitting the spin system. This assumption is conservative in the sense that spin contributions from the radicals would render larger intrinsic **g** anisotropies of the low-spin iron(III), which, on the other hand, would induce much larger anisotropic **A** tensor components than the observed one because of an "unquenched" orbital moment.

(22) (a) Griffith, J. S. *Proc. R. Soc. London* **1956**, *253*, 23. (b) Taylor, C. P. S. *Biochim. Biophys. Acta* **1977**, *491*, 137.

(23) The best solution in the model of Griffith and Taylor is obtained with $\Delta/\lambda = 20.7$ and $|V/\lambda| = 9.8$. The resulting **A** tensor would be proportional to $(-0.03, -0.88, -0.13)$ if the hole is in the *xz* orbital; the corresponding EFG tensor would also have its major component in the *y* direction.

(24) (a) Oosterhuis, W. T.; Lang, G. *Phys. Rev.* **1969**, *178*, 439. (b) Huynh, B. H.; Emptaage, M. H.; Münck, E. *Biochim. Biophys. Acta* **1978**, *534*, 295.

respectively. Hence, the main component of the EFG of the ligand quadrupole interaction can be expected essentially in the *z* direction.

On the other hand, the main contribution to the anisotropic *magnetic* hyperfine interaction should originate from spin−dipolar contributions induced by the *anisotropic spin-density distribution* in the ligand p shell. In a basic ligand field model, however, the three magnetic iron orbitals d_{z^2}, d_{xz}, and d_{yz} that interact with the p orbitals carry one unpaired electron each because of the intermediate-spin electron configuration $3d_{x^2-y^2}{}^0(3d_{z^2}3d_{xz}3d_{yz})^3 3d_{xy}{}^2$ that can be anticipated for the weak axial-ligand field. Hence, the spin-density distribution in the p shell should virtually resemble the charge anisotropy and, hence, the EFG and **A** tensors should be collinear for the apical ligands. However, the complexes **11a**−**c** are radical compounds, and we can assume that the "β" spin density of the two antiferromagnetically coupled equatorial-ligand radicals is partly transferred into the "α"-spin-carrying d_{xz} and d_{yz} orbitals by π interaction and reduces the net spin density of those iron orbitals. Furthermore, the effect can be very different for d_{xz} and d_{yz} if the ligand radicals are more concentrated at the equatorial sulfur than at the nitrogen, for instance. As a consequence, the spin density induced in the *apical* halide p_x and p_y orbitals also might be significantly different, which means that the magnetic anisotropy becomes significantly different from the charge anisotropy.

If this interpretation of the misalignment of EFG and **A** tensors at the *halogenide ligands* is basically correct, the appearance of strong quadrupole perturbation of the ligand hyperfine pattern in the EPR spectra provides another direct indication of ligand radicals. We mention that, to our knowledge, such strong *ligand* quadrupole effects have not been observed for iron compounds to date. According to our present understanding, this is not because of vanishing small EFGs but due to the usual collinear alignment of the EFG and **A** tensors, which prevents significant nuclear-level mixing in contrast to the situation of the present radical complexes.

In summary, the spectroscopic data corroborate the ferric nature of the compounds **11a**−**c** with *intermediate* spin $S_{Fe} = {}^3/_2$ and the presence of two radical ligands. The structure of the total spin ground state $S_t = {}^1/_2$ is characterized by antiferromagnetic alignment [↓($S = {}^1/_2$), ↑($^3/_2$), ↓($^1/_2$)], which is likely due to a strong antiferromagnetic iron−ligand exchange interaction that in this case dominates the inferior radical−radical interaction.

Conclusion

We have shown in this study that the air oxidation of ferrous complexes containing aminothiophenolato ligands yields ferric species with N,S-coordinated *o*-iminothionebenzosemiquinonate(1−) π radical ligands. In contrast to earlier literature reports,[6,7] we have not found spectroscopic evidence for the occurrence of iron(IV) ($S_{Fe} = 1$) or iron(V) ($S_{Fe} = {}^3/_2$ or $^1/_2$). The electronic structures of the resulting complexes are often complicated and were elucidated by a combination of electronic, EPR, and Mössbauer spectroscopies, X-ray crystallography, and magnetic-susceptibility measurements. The most salient results may be summarized as follows.

(1) The air oxidation of $[Fe^{III}(L^{AP})(L^{IP})]_2$ (**5a** or **5b**) or **2** and **3** yields the dinuclear complexes **6**−**8**, all of which contain two intermediate-spin ferric ions ($S_{Fe} = {}^3/_2$) that are intramolecularly antiferromagnetically coupled ($S_t = 0$). All of them (**6** and **7**) contain two terminal N,S-coordinated $(L^{ISQ})^{\bullet -}$ π radicals and a bridging $(L^{IP})^{2-}$ ligand, whereas **8** contains two $(^{\prime}N_2S_2^{\bullet\prime})^{3-}$ ligands.

(2) Complexes **6**−**8** under anaerobic conditions undergo addition reactions with phosphines, phosphites, or cyanide ligands yielding the diamagnetic five-coordinate mononuclear species $[Fe^{II}(L^{ISQ})_2(X)]^{n-}$ [X = $P(OPh)_3$, $n = 0$ (**9**); X = CN^-, $n = 1$ (**10**)], $[Fe^{II}(^{\prime}N_2S_2^{\bullet\bullet\prime})(PPh_3)]$,[6] and $[Fe^{II}(^{\prime}N_2S_2^{\bullet\bullet\prime})(P(n\text{-}Pr)_3)]$. These compounds contain a low-spin ferrous ion ($S_{Fe} = 0$) and two N,S-coordinated π radical ligands, $(L^{ISQ})^-$,that are antiferromagnetically coupled, yielding the observed $S_t = 0$ ground state.

(3) The reaction of **6** with stronger oxidants than air such as I_2, Br_2, and Cl_2 yields the dark-violet complexes **11a**−**c**. $[Fe^{III}(^{\prime}N_2S_2^{\bullet\bullet\prime})I]$ has been described in ref 7, where its crystal structure clearly revealed the presence of two *o*-iminothionebenzosemiquinonate π radicals. All of these mononuclear, five-coordinate compounds possess an $S_t = {}^1/_2$ ground state, which is shown to be attained by a strong intramolecular, antiferromagnetic coupling between an intermediate-spin ferric ion ($S_{Fe} = {}^3/_2$) and two N,S-coordinated *o*-iminothionebenzosemiquinonate π radicals. The EPR and Mössbauer spectroscopies of these species rule out unambiguously the alternative description invoking a low-spin ferric ion (and two ligand radicals).

Acknowledgment. We thank the Alexander von Humboldt Foundation for a fellowship to P.G. We are grateful to the Fonds der Chemischen Industrie for financial support.

Supporting Information Available: X-ray crystallographic files, in CIF format, for compounds **6**−**9**. This material is available free of charge via the Internet at http://pubs.acs.org.

JA021409M